

Controlling Aggregation in Highly Emissive Pt(II) Complexes Bearing Tridentate Dianionic N[^]N[^]N Ligands. Synthesis, Photophysics, and Electroluminescence

Mathias Mydlak,[†] Matteo Mauro,[†] Federico Polo,[†] Michael Felicetti,[‡] Jens Leonhardt,[‡] Gerhard Diener,[‡] Luisa De Cola,^{*,†} and Cristian A. Strassert^{*,†}

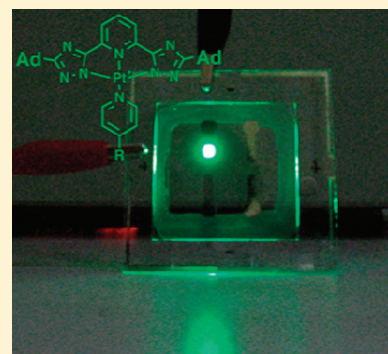
[†]Physikalisches Institut and Center for Nanotechnology (CeNTech), Westfälische Wilhelms-Universität Münster, Mendelstrasse 7, D-48149 Münster, Germany

[‡]Sensient Imaging Technologies GmbH, Chemie Park Bitterfeld-Wolfen, Areal A, Sensientstrasse 3, 06766 Bitterfeld-Wolfen, Germany

S Supporting Information

ABSTRACT: Neutral Pt(II) complexes bearing tridentate dianionic 2,6-bis(1*H*-1,2,4-triazol-5-yl)pyridine and ancillary alkyl-substituted pyridine ligands have been synthesized and characterized. They show bright green emission, reaching 73% photoluminescence quantum yield in deaerated chloroform solution, which can be assigned to a predominantly metal-perturbed ligand-centered phosphorescence. We have followed two strategies to preserve the spectral purity of the monomeric species by varying the substituents on the chromophoric or on the ancillary ligands. However, variations in the substitution patterns only modestly affected the radiative and radiationless deactivation rate constants of the monomers. Photophysical and electrochemical properties have been measured for all the complexes and correlated with calculations using time-dependent density functional theory. The electroluminescence spectra of the brightest, nonaggregating derivative showed a better color purity than that of iridium(III) tris(phenylpyridine), thus proving that aggregation was hindered in a running electroluminescent device.

KEYWORDS: platinum(II) complexes, tridentate ligand, green emission, 1,2,4-triazoles



1. INTRODUCTION

The search for electroluminescent metal complexes without the relatively scarce iridium has led to several classes of emitters based on transition metals such as rhenium,^{1–4} osmium,^{5–8} platinum^{9–33} or gold^{34,35} or on cheaper and less toxic ones, e.g., copper^{36–38} and zinc.^{39–51}

Pt(II) complexes have also been recently considered as triplet emitters. They have a d^8 electronic configuration and, as a result, exhibit a square planar coordination geometry, which makes them prone to formation of aggregates or excimers, originating shifts in the emission and influencing the photoluminescence quantum yields (PLQYs).^{13,16,52} Although this can be advantageous for the realization of white organic light-emitting diodes (WOLEDs), it also represents a drawback for applications where color purity is desired.^{11,12,15,33} Terpyridine ligands^{53–56} and their N[^]C[^]N and N[^]N[^]C analogues have been coordinated to Pt(II),^{18,19,24,57–61} yielding neutral or singly or doubly charged complexes, some of them showing bright luminescence. We have recently reported a straightforward one-pot synthesis of neutral, soluble Pt(II) coordination compounds bearing a dianionic tridentate ligand. The coordination of an alkylpyridine ancillary moiety to the 2,6-bis(triazolyl)pyridine-based complex allowed us to enhance the solution processability, reaching 87% PLQY in thin films.⁶² Unfortunately, this derivative is only able to emit yellow

light when assembled into the emitting aggregates. Furthermore, the nitrogen-rich tetrazole rings make it thermally unstable and, therefore, unsuitable for vapor-processed devices.^{63–66}

To control aggregation, which leads to undesired broadening of spectra, and to replace the decomposing tetrazole rings, we have designed and synthesized a new class of neutral Pt(II) complexes bearing tridentate dianionic 2,6-bis(1*H*-1,2,4-triazol-5-yl)pyridine chelates and ancillary alkyl-substituted pyridine ligands. 1,2,4-triazoles can be conveniently functionalized at the C3 position to tune the emission and aggregation properties and possess a strong σ donating character that favors luminescence.

Tuning of color, aggregation, and processability are key parameters for applications in electroluminescent devices. Therefore, the substitution pattern of the triazole rings was varied by the alternative introduction of bulky, aliphatic adamantyl groups or conjugated, aromatic tolyl moieties, and their influence is discussed in detail. The photophysical properties have been investigated and supported by computational calculations, and vapor-processed devices were prepared with the most promising derivative, displaying an electroluminescence spectrum with no

Received: April 15, 2011

Revised: June 24, 2011

Published: July 22, 2011

evidence of aggregation and, consequently, even better color purity than iridium(III) tris(phenylpyridine) (hereafter Ir(ppy)₃).

2. EXPERIMENTAL SECTION

2.1. Experimental Techniques. *2.1.1. Photophysics.* Absorption spectra were measured on a Varian Cary 5000 double-beam UV–vis–NIR spectrometer and baseline corrected. Steady-state emission spectra were recorded on an Edinburgh FS920 spectrometer equipped with a 450 W xenon-arc lamp, excitation and emission monochromators (1.8 nm/mm dispersion, 1800 grooves/mm blazed at 500 nm), and a Hamamatsu R928 photomultiplier tube. Emission and excitation spectra were corrected for source intensity (lamp and grating) by standard correction curves. Time-resolved measurements were performed using the multichannel scaling (MCS) single-photon-counting option on the HORIBA Jobin-Yvon IBH FL-322 Fluorolog 3. A pulsed xenon lamp was used to excite the sample. The excitation sources were mounted directly on the sample chamber at 90° to a double-grating emission monochromator (2.1 nm/mm dispersion, 1200 grooves/mm) and collected by a TBX-4-X single-photon-counting detector. The photons collected at the detector are correlated by a time-to-amplitude converter (TAC) to the excitation pulse. Signals were collected using an IBH Data Station Hub photon-counting module, and data analysis was performed using the commercially available DAS6 software (HORIBA Jobin Yvon IBH). The quality of the fit was assessed by minimizing the reduced χ^2 function and by visual inspection of the weighted residuals.

All solvents were spectrometric grade. Deaerated samples were prepared by the freeze–pump–thaw technique.

2.1.2. UV Photoelectron Spectroscopy (UPS). UPS was measured on a Riken Keiki AC-2 system using the low-energy electron counter method with a deuterium lamp as the light source and a grating type monochromator as the spectrometer.

2.1.3. Computational Details. Geometries were optimized by means of density functional theory (DFT). The parameter-free hybrid functional Perdew–Burke–Erzenhof^{67–69} was employed along with the standard valence double- ζ polarized basis set 6-31G(d,p)⁷⁰ for C, H, F, and N. For Pt, the Stuttgart–Dresden (SDD) effective core potentials were employed along with the corresponding valence triple- ζ basis set. All the calculations were done assuming C_s symmetry. The nature of all the stationary points was checked by computing vibrational frequencies, and all the species were found to be true potential energy minima, as no imaginary frequency was obtained (NImag = 0). To simulate the absorption electronic spectrum down to 250 nm, for each complex the lowest 20 singlet (S₀ → S_n) as well as the 3 lowest triplet (S₀ → T_n) excitation energies were computed on the optimized geometry at S₀ by means of time-dependent density functional theory (TD-DFT) calculations.^{71,72} Oscillator strengths were deduced from the dipole transition-matrix elements (for single states only). All the calculations were performed in vacuum and with the Gaussian 09 program package.⁷³

2.1.4. Electrochemistry. The electrochemical characterization (cyclic voltammetry) for the metal complexes herein reported was performed in methylene chloride (dichloromethane, DCM)/0.1 M tetrabutylammonium hexafluorophosphate (TBAH). The concentration of the samples was 0.5 mM. Glassy carbon was employed as the working electrode, platinum wire as the counter electrode, and silver wire as the quasi-reference electrode (QRE). DCM (Acros Organics, 99.8%, extra dry over molecular sieves) was used as received without any further purification. TBAH (electrochemical grade, ≥99%, Fluka) was used as the supporting electrolyte, which was recrystallized from a 1:1 ethanol–water solution and dried at 60 °C under vacuum.

For the electrochemical experiments, a CHI750C electrochemical workstation (CH Instruments, Inc., Austin, TX) was used. The electrochemical experiments were performed in a glass cell under an Ar atmosphere. To minimize the ohmic drop between the working and

the reference electrodes, the feedback correction was employed. The electrochemical experiments were performed by using a homemade 3 mm diameter glassy carbon disk electrode (from a glassy carbon rod, Tokai Inc.). The working electrodes were stored in ethanol and before the experiments were polished with a 0.05 μm diamond suspension (Metadi Supreme Diamond Suspension, Buehler) and ultrasonically rinsed with ethanol for 5 min. The electrode was electrochemically activated in the background solution by means of several voltammetric cycles at 0.5 V s⁻¹ between the anodic and cathodic solvent/electrolyte discharges until the same quality features were obtained. The reference electrode was a silver quasi-reference electrode (Ag-QRE), which was separated from the catholyte by a glass frit (Vycor). The reference electrode was calibrated at the end of each experiment against the ferrocene/ferricenium couple, whose formal potential is 0.460 V against the KCl saturated calomel electrode (SCE); in the following, all potential values are reported against the SCE. A platinum ring or coil served as the counter electrode.

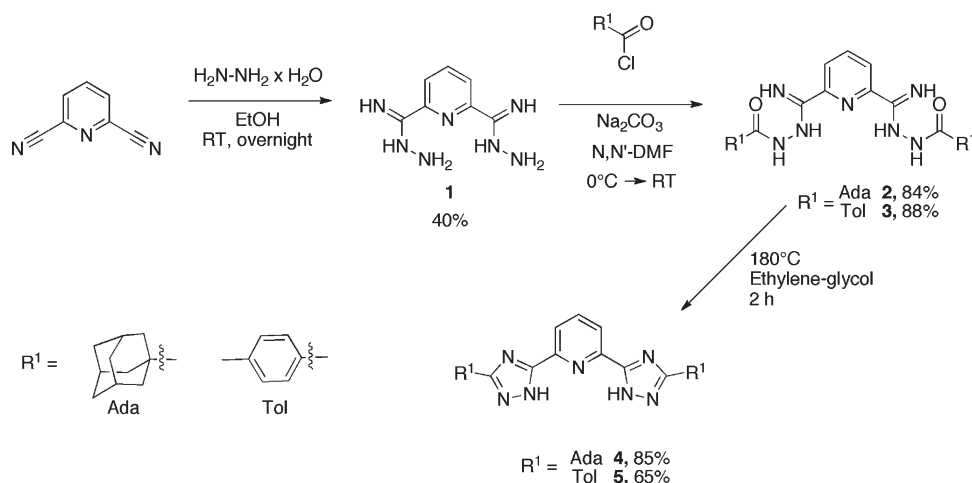
2.1.5. Device Preparation. All layers were prepared by thermal evaporation in a high-vacuum system with a pressure of less than 10⁻⁴ Pa without breaking the vacuum. ITO-coated glass plates with a surface resistivity of ≤15 Ω/\square were used as substrates. They were ultrasonically cleaned and treated with oxygen plasma for work function tuning and chemical cleaning. During the evaporation, the deposition rates were monitored by controllers, which were calibrated using a Dektak 6 M profiler. The deposition rate was 0.1 nm/s, and the layer thickness was checked by quartz balances. The *J–V–L* characteristics were measured by using a Keithley 238 (high-current source measure unit) and Keithley 2000 (multimeter) with a calibrated silicon photodiode under nitrogen. Spectra were recorded on a tec5 spectrometer unit LOE-USB. The luminance values were measured at normal incidence, and the total flux was estimated by assuming a Lambertian distribution.

2.1.6. Synthesis and Characterization. All reagents were analytical grade and used as received. Column chromatography (CC) was performed with silica gel 60 (particle size 63–200 μm , 230–400 mesh, Merck). NMR spectra were recorded on an ARX 300 or an AMX 400 from Bruker Analytische Messtechnik (Karlsruhe, Germany). The ¹H NMR chemical shifts (δ) of the signals are given in parts per million and referenced to residual protons in the deuterated solvents: chloroform-*d*₁ (7.26 ppm), dimethyl sulfoxide-*d*₆ (2.50 ppm), or methylene chloride-*d*₂ (5.32 ppm). The signal splittings are abbreviated as follows: s, singlet; d, doublet; t, triplet; q, quartet; m, multiplet. All coupling constants (*J*) are given in hertz. Mass spectrometry was performed in the Department of Chemistry, University of Münster. Electrospray ionization (ESI) mass spectra were recorded on a Bruker Daltonics (Bremen, Germany) MicroToF with loop injection. Elemental analysis was recorded at the University of Milan, Italy.

2.2. Synthesis. *2.2.1. Pyridine-2,6-bis(carboximidhydrazide) (1).* To a solution of 2,6-pyridinedicarbonitrile (20 g, 0.155 mol) in ethanol (1 L) was added hydrazine monohydrate (151 mL, 3.1 mol). The reaction mixture was stirred at room temperature (rt) overnight, yielding a pale yellow precipitate in a yellow solution. The precipitate was filtered off, washed with cold ethanol, and dried (12 g, 40%). ¹H NMR (300 MHz, dimethyl sulfoxide (DMSO)): δ 7.82 (d, *J* = 0.8 Hz, 1H), 7.80–7.78 (m, 2H), 7.65 (dd, *J* = 8.5, 7.1 Hz, 2H), 6.07 (s, 4H), 5.28 (s, 4H). MS (ESI+, MeOH, *m/z*): calcd for [M + H]⁺, 194.11487; found, 194.11472 ([M + H]⁺).

2.2.2. N,N''-(Pyridine-2,6-diylbis(iminomethylene))bis(adamantane-1-carbohydrazide) (2). A flame-dried, nitrogen-purged Schlenk tube was loaded with **1** (5 g, 26 mmol) and sodium carbonate (6.1, 58 mmol), evacuated, gently heated, and refilled with nitrogen after being cooled to rt. Next, dry *N,N*-dimethylformamide (*N,N*-DMF; 160 mL) was added, and the suspension was cooled to 0 °C. In a separately prepared Schlenk tube, a 1-adamantanecarbonyl chloride (10.3 g, 52 mmol) solution in dry *N,N*-DMF (60 mL) was prepared the same way as above. This solution

Scheme 1. General Synthetic Procedure for Compounds 1–5



was then slowly added to the cooled suspension under strong stirring. The pale yellow suspension cleared for some time to a darker yellow solution, except for the sodium carbonate, followed by the precipitation of a yellow solid overnight while the reaction mixture was allowed to warm to rt. Then the reaction volume was doubled by the addition of water, yielding more precipitate. This suspension was stirred strongly for another 1.5 h and then filtered and washed with water thoroughly. The yellow solid was dried under vacuum and used as is for the next step. (11 g, 84%).

2.2.3. *N,N''*-(Pyridine-2,6-diylbis(iminomethylene))bis(4-methylbenzohydrazide) (**3**). The synthesis was similar to the preparation of **2** using *p*-tolyl chloride. The product was pale yellow (10 g, 88%).

2.2.4. 2,6-Bis(3-((3*R*,5*R*,7*R*)-adamantan-1-yl)-1*H*-1,2,4-triazol-5-yl)pyridine (**4**). Product **2** was suspended in ethylene glycol in a 1 mL/100 mg ratio in an open round-bottom flask. This suspension was heated to 180 °C, eliminating water. Once the solution was clear, the reaction mixture was heated under reflux for another hour. After the reaction mixture was cooled to rt, the product was precipitated with water and stirred strongly for 1 h more. The white solid was filtered, washed with water, and dried under vacuum (8.5 g, 85%). ¹H NMR (300 MHz, DMSO): δ 8.08 (s, 2H), 8.07–7.99 (m, 1H), 4.50 (s, 2H), 2.05 (s, 6H), 2.02 (s, 12H), 1.76 (s, 12H). MS (ESI+, MeOH, *m/z*): calcd for [M + H]⁺, 482.30; found, 482.3026 ([M + H]⁺).

2.2.5. 2,6-Bis(3-*p*-tolyl)-1*H*-1,2,4-triazol-5-yl)pyridine (**5**). The preparation was similar to that of **4**, starting from **3**. (6 g, 65%). ¹H NMR (300 MHz, DMSO): δ 14.50 (s, 2H), 8.26–8.09 (m, 4H), 8.03 (dd, *J* = 8.1, 3.1 Hz, 3H), 7.34 (d, *J* = 7.0 Hz, 4H), 2.38 (s, 6H). MS (ESI+, MeOH, *m/z*): calcd for [M + H]⁺, 394.18; found, 394.1775 ([M + H]⁺); calcd, for [M + Na]⁺, 416.43; found, 416.1593 ([M + Na]⁺).

2.2.6. General Procedure for the Synthesis of the Pt(II) Complexes **6a**, **6b**, **7a**, and **7b**. The tridentate ligand (1.1 equiv), PtCl₂·(DMSO)₂, and the solvent mixture (2-methoxyethanol/water, 3:1) were placed in a round-bottom flask. The according alkyl-substituted pyridine derivative was added, and the mixture was then heated to 83 °C under nitrogen overnight. The precipitation of the product started within 30 min. After the solution was cooled to rt, its volume was doubled by adding water to precipitate all the product. It was collected by filtration, washed with water, and dried. The crude product was then dissolved in DCM and adsorbed onto neutral alumina. This was loaded onto a column packed with neutral alumina, and a column chromatographic separation was performed using DCM/methanol (99:1) as the eluent. The first fraction was the product, which was collected and dried. After that, it was dissolved

in a small amount of DCM and precipitated with hexane. The fine precipitate was collected via centrifugation and dried under vacuum. Overall yields after purification were close to 10%.

Data for 6a. ¹H NMR (400 MHz, CD₂Cl₂): δ 10.01 (dd, *J* = 5.4, 1.3 Hz, 2H), 7.87 (dd, *J* = 8.1, 7.7 Hz, 1H), 7.58 (d, *J* = 7.9 Hz, 2H), 7.43 (d, *J* = 6.7 Hz, 2H), 2.81–2.70 (m, 2H), 2.10 (s, 14H), 1.82 (s, 12H), 1.74 (s, 3H), 1.57 (s, 6H), 1.42–1.33 (m, 4H). ¹³C NMR (75 MHz, CD₂Cl₂): δ 171.92 (s), 163.16 (s), 156.54 (s), 154.13 (s), 150.91 (s), 142.76 (s), 126.59 (s), 116.23 (s), 42.50 (s), 37.47 (s), 35.93 (s), 35.84 (s), 31.86 (s), 30.03 (s), 29.37 (s), 22.98 (s), 14.26 (s). MS (ESI+, MeOH, *m/z*): calcd for [M + H]⁺, 824.37; found, 824.3721 ([M + H]⁺); calcd for [M + Na]⁺, 846.35; found, 846.3505 ([M + Na]⁺). Anal. Calcd for C₃₉H₄₈N₈Pt: C, 56.85; H, 5.87; N, 13.60. Found: C, 56.51; H, 5.73; N, 13.53.

Data for 6b. ¹H NMR (300 MHz, CD₂Cl₂): δ 10.15 (d, *J* = 6.9 Hz, 2H), 7.85 (s, 1H), 7.60 (d, *J* = 7.9 Hz, 2H), 7.54 (d, *J* = 7.0 Hz, 2H), 2.12 (s, 12H), 2.11–2.06 (m, 6H), 1.84 (s, 12H), 1.79–1.69 (m, 6H), 1.32–1.25 (m, 6H), 1.13–0.98 (m, 6H), 0.88 (t, *J* = 7.3 Hz, 9H). ¹³C NMR (75 MHz, CD₂Cl₂): δ 171.23 (s), 162.82 (s), 162.17 (s), 153.52 (s), 150.37 (s), 142.24 (s), 124.62 (s), 116.02 (s), 44.53 (s), 42.37 (s), 37.34 (s), 36.97 (s), 35.65 (s), 29.33 (d, *J* = 15.1 Hz), 26.04 (s), 23.77 (s), 14.21 (s). MS (ESI+, MeOH, *m/z*): calcd for [M + H]⁺, 936.50; found, 936.4994 ([M + H]⁺). Anal. Calcd for C₄₇H₆₄N₈Pt·0.5CH₂Cl₂: C, 58.30; H, 6.69; N, 11.45. Found: C, 58.19; H, 6.43; N, 12.11.

Data for 7a. ¹H NMR (400 MHz, CD₂Cl₂): δ 9.82 (d, *J* = 6.6 Hz, 2H), 8.01 (t, *J* = 11.0 Hz, 4H), 7.56–7.50 (m, 1H), 7.43 (d, *J* = 7.5 Hz, 2H), 7.28 (d, *J* = 7.9 Hz, 4H), 7.21 (d, *J* = 6.4 Hz, 2H), 2.43 (s, 6H), 1.49 (s, 2H), 1.31 (ddd, *J* = 22.7, 15.5, 8.5 Hz, 6H), 0.92 (t, *J* = 7.1 Hz, 3H). ¹³C NMR (ESI+, CHCl₃, *m/z*): calcd for [M + H]⁺, 736.25; found, 736.24929 ([M + H]⁺). Anal. Calcd for C₃₃H₃₂N₈Pt·0.5CH₂Cl₂: C, 51.20; H, 4.27; N, 14.40. Found: C, 50.93; H, 3.9; N, 14.66.

Data for 7b. ¹H NMR (300 MHz, CD₂Cl₂): δ 10.17–10.12 (m, 2H), 8.12 (d, *J* = 8.1 Hz, 4H), 7.99–7.94 (m, 1H), 7.73 (d, *J* = 8.0 Hz, 2H), 7.65–7.59 (m, 2H), 7.29 (d, *J* = 7.9 Hz, 4H), 2.42 (s, 6H), 1.74 (s, 6H), 1.34–1.28 (m, 6H), 1.09 (s, 6H), 0.90 (t, *J* = 7.3 Hz, 9H). ¹³C NMR (75 MHz, CD₂Cl₂): δ 164.24 (s), 162.69 (s), 161.80 (s), 153.47 (s), 150.18 (s), 142.77 (s), 138.96 (s), 130.42 (s), 129.72 (s), 126.55 (s), 124.89 (s), 116.75 (s), 44.72 (s), 37.12 (s), 26.20 (s), 23.93 (s), 21.72 (s), 14.40 (s). MS (ESI+, CHCl₃, *m/z*): calcd for [M + H]⁺, 848.37; found, 848.37243 ([M + H]⁺); calcd for [M + Na]⁺, 870.35; found 870.35567 ([M + Na]⁺). Anal. Calcd. for C₄₁H₄₈N₈Pt·CH₂Cl₂: C, 54.07; H, 5.40; N, 12.01. Found: C, 53.25; H, 5.56; N, 13.24.

Scheme 2. Synthesis of Complexes 6a, 6b, 7a, and 7b

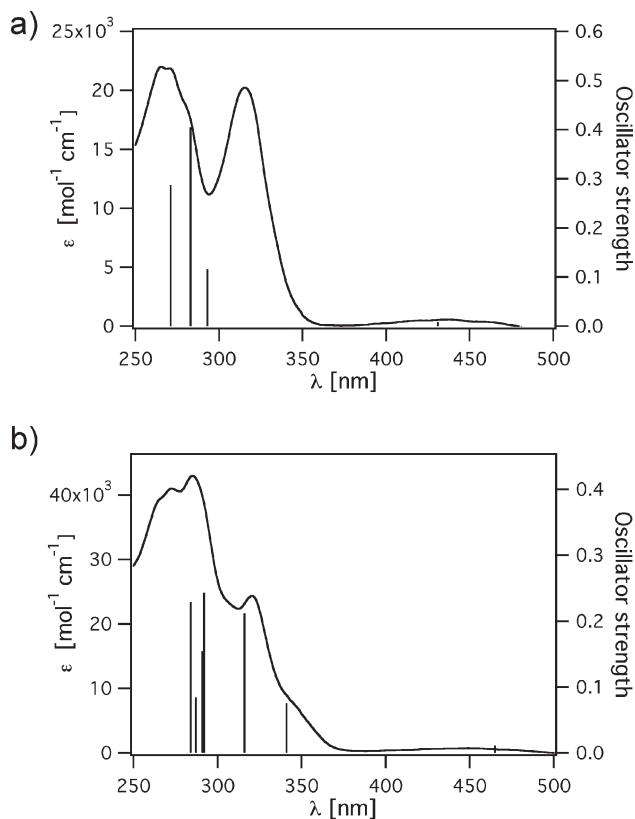
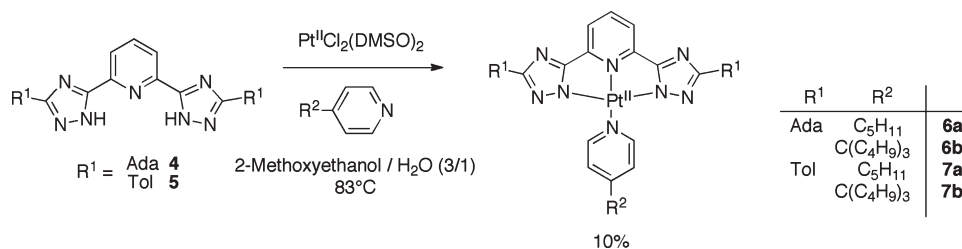


Figure 1. Absorption spectra of **6a** (a) and **7a** (b) in chloroform solutions. Calculated absorption peaks in vacuum are shown for comparison.

3. RESULTS AND DISCUSSION

3.1. Synthesis. A general overview of the synthetic strategy is depicted in Scheme 1.

Starting from 2,6-pyridinedicarbonitrile, the bisamidrazone **1** is obtained upon reaction with hydrazine monohydrate. This intermediate **1** is further reacted with the corresponding acyl chloride, either adamantancarboxylchloride to yield **2** or *p*-tolylcarbonyl chloride, leading to **3**. These are the direct precursors to the substituted 1,2,4-triazoles, which are formed in a condensation reaction in ethylene glycol at 180 °C.⁷⁵ The tridentate ligands **4** and **5** and the ancillary pyridine derivatives were reacted with $PtCl_2(DMSO)_2$, yielding complexes **6a**, **6b**, **7a**, and **7b**, as can be seen in Scheme 2. It is interesting to notice that only the one-pot approach yields the desired products upon purification by column chromatography and crystallization. Attempts to first coordinate the tridentate ligand and to leave a labile solvent molecule only

lead to insoluble, nonluminescent products, as previously reported for our analogous bistetrazolylplatinum(II) complexes.⁶²

Complexes **6a** and **6b** are more soluble in chlorinated solvents than the tolyl-terminated ones due to the two bulky adamantyl substituents on the triazoles. To further enhance the solubility without affecting the emission color, we introduced either a linear (C5) or a branched (C13) alkyl substituent in the 4-position on the ancillary pyridine ligand. Complexes **6a** and **6b** are both soluble in chloroform, and the branched tail was especially useful to enhance the solubility of **7b**, if compared with **7a**. The complexes have been characterized by high-resolution mass spectrometry, ¹H and ¹³C NMR spectroscopy, and elemental analysis (see the Experimental Section and Figure S1, Supporting Information).

3.2. Absorption Spectroscopy and Frontier Orbitals. The absorption spectra of complexes **6a** and **7a** in chloroform are depicted in parts a and b, respectively, of Figure 1 (for the sake of clarity, the similar absorption spectra of **6b** and **7b** are shown in the Supporting Information, Figure S2). The molar absorption coefficients are collected in Table 1.

Complexes **6a** and **7a** were also investigated by means of DFT, and the corresponding computational data are summarized in Tables S1 and S2 of the Supporting Information. Their ground-state geometries were optimized (see parts a and b, respectively, of Figure S3, Supporting Information), along with other substitution patterns on the triazole moieties (namely methyl, hydrogen, and phenyl, parts a, b, and c, respectively, of Figure S4, Supporting Information), to verify a significant correlation with the calculated frontier orbitals (see Figure S5, Supporting Information) and geometries obtained by DFT.

Moreover, to gain deeper insight into the nature of the electronic transitions involved in the absorption spectra, the complexes were investigated by using TD-DFT and the computed vertical transitions described in terms of molecular orbitals of the corresponding ground-state geometry. The calculated energies are listed in Table S3, Supporting Information, together with the nature of the involved orbitals and their expansion coefficients. It can be seen that they nicely agree with the experimental values (see Figure 1; further computational details can be found in the Experimental Section).

The experimental spectra clearly show a broad and featureless weak band ($\epsilon = 0.49\text{--}0.91 \times 10^3 \text{ M}^{-1} \text{ cm}^{-1}$) between 400 and 500 nm, which can be attributed to the energetically lowest lying metal-to-ligand charge-transfer (MLCT) transitions, as already observed for comparable compounds.⁶⁰ These bands are the $S_0 \rightarrow S_1$ transitions and mainly involve the platinum d orbitals (partially mixed with the tridentate-ligand-centered π orbitals) and π^* orbitals of the chelate ($\text{HOMO} \rightarrow \text{LUMO}$). The more intense bands ($\epsilon = 1.1\text{--}4.3 \times 10^4 \text{ M}^{-1} \text{ cm}^{-1}$) observed at higher

Table 1. Photophysical Properties of Compounds 6a, 6b, 7a, and 7b

complex	λ_{abs} [nm] ($\epsilon \times 10^{-3}/$ [M ⁻¹ cm ⁻¹]) ^{a,b}	$\lambda_{\text{em}} \text{RT}^{a,b,c}$ [nm]	$\lambda_{\text{em},77 \text{ K}}^d$ [nm]	Φ_{em} aer ^{d,e,f}	Φ_{em} dear ^{d,e,f}	$\tau(\text{rt})$ deaer ^d [μs]	$\tau(\text{rt})$ aer ^d [μs]	$\tau(77 \text{ K})^d$ [μs]	$k_{\text{r}} \times 10^{-4}$ [s ⁻¹]	$k_{\text{nr}} \times 10^{-4}$ [s ⁻¹]
6a	265 (22), 316 (20), 420 (0.49)	507, 540 579 (sh)	493, 529, 569	0.02	0.73	14.14	0.39	14.59	5.13	1.95
6b	266 (33), 316 (30), 421 (0.91)	507, 539, 574 (sh)	493, 529, 568	0.02	0.64	13.62	0.42	14.19	4.69	2.65
7a	273 (41), 285 (43), 320 (24), 342 (8.6, sh), 433 (0.64)	530, 560, 608 (sh)	514, 555, 604	0.02	0.73	16.07	0.44	14.84 (39%) 3.48 (61%); ^f 13.59 (81%) 3.17 (81%); ^g	4.54	1.68
7b	272 (40), 283 (38), 321 (23), 338 (10.5, sh), 436 (0.71)	527, 560, 603 (sh)	513, 550, 593	0.01	0.67	15.64	0.32	17.72	4.28	2.11

^aIn chloroform. ^bThe abbreviation “sh” denotes a shoulder. ^c $\lambda_{\text{exc}} = 315 \text{ nm}$ (6a, 6b) and 320 nm (7a, 7b). ^dIn a 2-MeTHF matrix. ^eQuantum yields were measured in an integrating sphere system. ^fMonitored at $\lambda_{\text{em}} = 515 \text{ nm}$. ^gMonitored at $\lambda_{\text{em}} = 600 \text{ nm}$.

Table 2. Frontier Orbitals Obtained from Electrochemistry and UPS^a

complex	$E_{\text{ox}}(\text{HOMO})$	$E_{\text{red}}(\text{LUMO})$	$\Delta E_{\text{HOMO-LUMO}}$ (eV)	HOMO ^d (eV)
6a	+1.51 V ^b (−5.84 eV)	−1.64 V ^c (−2.69 eV)	3.15	−5.45
6b	+1.52 V ^b (−5.86 eV)	−1.61 V ^c (−2.72 eV)	3.14	−5.71
7a	+1.44 V ^b (−5.77 eV)	−1.56 V ^c (−2.78 eV)	2.99	−5.54
7b	+1.44 V ^b (−5.78 eV)	−1.55 V ^c (−2.79 eV)	2.99	−5.59

^aSamples of 0.5 mM concentration in DCM/0.1 M TBAH solutions were investigated. Glassy carbon was employed as the working electrode, a platinum ring as the counter electrode, and a silver wire as the reference electrode. The scan rate was varied in the range of 0.1–5 V s⁻¹. ^bIrreversible peak, $E = E_{\text{p}}$. ^cReversible peak, $E = E^{\circ}$, calculated as the mean value between the cathodic and the anodic peaks averaged in the scan rate range of 0.1–0.5 V s⁻¹. ^dThe HOMO levels of drop-casted neat films were measured by UPS.

energy (ca. 265–321 nm) can be described as spin-allowed, ligand-centered (LC) in nature, involving mainly the tridentate ligand ($\pi \rightarrow \pi^*$).

As far as complexes 7a and 7b are concerned, the absorption bands at about 340 nm can be ascribed to a transition with mixed MLCT/LC character (HOMO \rightarrow LUMO + 1, computed at 341 nm for 7a). Indeed, the HOMO of the tolyl-substituted triazole complexes extends beyond the triazole rings, also involving the tolyl substituents, while the LUMO + 1 is mostly localized on the pyridine moiety of the chelate (see Figure S5a, Supporting Information).

For complexes 6a and 6b, thus in absence of π -conjugated tolyl moieties, the lowest LC bands are observed at about 316 nm (Figure 1). They can be attributed to the $\pi-\pi^*$ transitions of the tridentate ligand without any contribution from the aliphatic substituents. Nevertheless, these transitions still display a slight MLCT character, as reflected by TD-DFT calculations (see Table S3 and Figure S5a, Supporting Information). Finally, the energetically higher bands are due to $\pi-\pi^*$ transitions involving the occupied orbital located on the triazole rings and the virtual orbital mainly located on the pyridine of the tridentate ligand (HOMO – 1 \rightarrow LUMO + 2, computed at 271 nm for 6a; see Figure S5c). Similar explanations can be adduced for the higher energy absorption bands displayed by 7a and 7b.

Electrochemical and UPS measurements were performed to experimentally estimate the HOMO and LUMO levels (Table 2). The results show that the introduction of conjugated moieties reduces the HOMO–LUMO gap as expected by destabilizing the HOMO and lowering the LUMO. Theoretical calculations support these observations, confirming that the destabilization of the HOMO is more pronounced than the stabilization of the LUMO (0.29 eV vs 0.10 eV, respectively; see Table S2, Supporting Information).

The redox processes were studied by varying the scan rate in the range of 0.1–5 V s⁻¹, and the peak currents were found to depend linearly on the square root of the scan rate as expected for a diffusion-controlled redox process.⁷⁶ The values are collected in Table 2; cyclic voltammograms are shown in the Supporting Information (see Figures S6 and S7). The electrochemical behavior in dichloromethane of the two pairs 6a/6b and 7a/7b showed similar patterns in the negative bias, i.e., a reversible peak in the potential range from –1.55 to –1.64 V. The first reduction process for 6a and 6b (–1.64 V) occurs at a more negative potential than the same process for complexes 7a and 7b (–1.55 V).

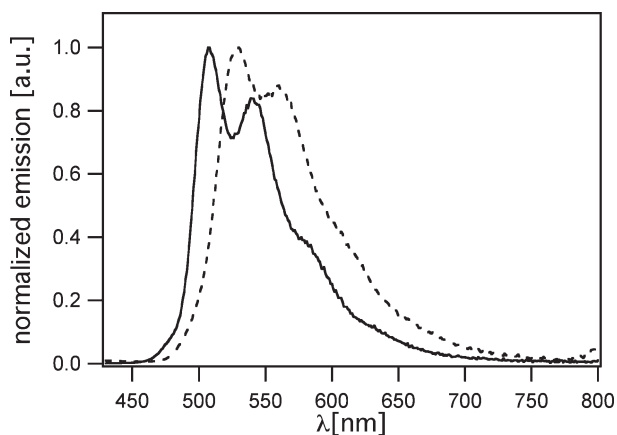


Figure 2. Emission spectra of **6a** (solid line) and **7a** (dashed line) in degassed chloroform solutions ($\lambda_{\text{exc}} = 315$ nm for **6a** and 320 nm for **7a**).

However, this small difference represents only a weak modulation, which indicates that the LUMO is mainly centered on the pyridine moiety of the tridentate ligand. This evidence is also supported by computational calculations (see Table S2 and Figure S5a).

In the positive bias, an irreversible oxidation wave is observed in the range between +1.44 and +1.52 V and is mainly related to the oxidation of the metal core.^{10,11,16,19,24,27,29,32,53,59,61,77–82}

The results show that a shift is observed upon a change of the functional group on the triazole moieties of the tridentate ligand. This can be rationalized taking into consideration that the triazole moieties contribute to the HOMO of the complexes. If they exclusively involved the d orbitals of the Pt center, they would be less sensitive to the change of the triazole substituents.

3.3. Photophysics. Complexes **6a** and **6b** show emission spectra peaking at 509 nm in chloroform at room temperature, whereas **7a** and **7b** emit at 530 nm (see Figure 2 and Figures S8–S10 in the Supporting Information). To simulate the phosphorescent spectra, the vertical (Franck–Condon) excitation energies from the optimized ground state (S_0) to the lowest lying triplet manifold (T_1) were computed at the TD-DFT level. Indeed, this method has been already successfully used for other phosphorescent platinum complexes.^{83,84} The $S_0 \rightarrow T_1$ transitions display mainly HOMO \rightarrow LUMO character and were calculated at 481 and 526 nm for **6a** and **7a**, respectively, in good agreement with the experimental values (see Table 1 and Table S3 in the Supporting Information).

This red shift relative to the adamantyl-substituted compounds can be rationalized considering the extended conjugation caused by the aromatic substitution on the triazole ligand, which leads to a smaller HOMO–LUMO separation (vide supra), i.e., a lower emission energy. Extended conjugation would also account for the slightly lower radiative rate constants of compounds **7a** and **7b**, if compared with their adamantyl-substituted analogues **6a** and **6b**, respectively (see Table 1). On the other hand, the radiationless deactivation is slightly slower for the comparatively rigid aromatic moieties (see Table 1). All in all, the excited-state lifetime is somewhat longer for tolyl-substituted complexes.

In chloroform solution, both classes of complexes display emissions from excited states with mainly ^3LC character, which correlates with the observed vibrational progression, long excited-state lifetimes, and sensitivity to quenching by oxygen. The PLQYs are remarkably high, above 65%, reaching 73% for **6a** and **7a**,

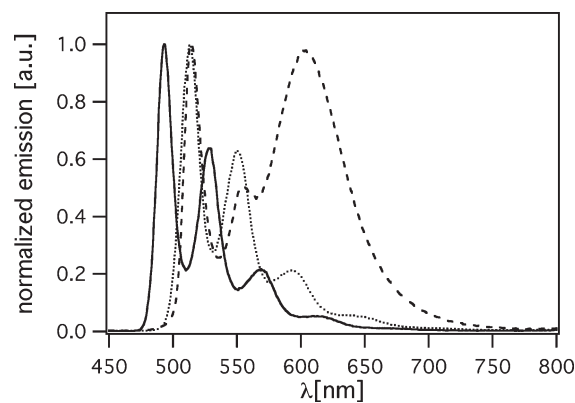


Figure 3. Emission spectra of **6a** (solid line), **7a** (dashed line), and **7b** (dotted line) in 2-MeTHF glass matrixes at 77 K ($\lambda_{\text{exc}} = 305$ nm for **6a** and 310 nm for **7a** and **7b**).

which, to the best of our knowledge, represents the highest value reported so far for $\text{N}^{\wedge}\text{N}^{\wedge}\text{N}$ Pt(II) coordination compounds and among the highest for tridentate chelates.^{18,19,24,53–61} A summary of the photophysical data is shown in Table 1.

At room temperature, the complexes show identical emission energies within the same family of compounds, i.e., **6a** and **6b** or **7a** and **7b**. The lack of noticeable shifts within the emission spectra in frozen 2-MeTHF matrixes at 77 K (see Table 1, Figure 3, and Figure S11–S13 in the Supporting Information) is indicative of the weak $^3\text{MLCT}$ character of the emissive excited state, which is mainly ^3LC , as can be deduced from the clear vibrational progression and long excited-state lifetimes. The only exception is represented by **7a**, which in frozen matrixes displays an additional broad, unstructured, and red-shifted emission band centered around 605 nm. This dual emission can be explained by the formation of emissive aggregates. Therefore, the structured emission of the monomeric form displaying a clear vibrational progression is observed along the featureless band of the aggregates at lower energy, leading also to biexponential excited-state lifetimes. The longer component (13.6 μs) corresponds to the monomer and the shorter one (3.2 μs) to the aggregated species (see Table 1).

Ground-state aggregation is evidenced by the broad additional metal–metal-to-ligand charge-transfer (MMLCT) band in the excitation spectrum of the red-shifted band and cannot be observed when monitoring the monomeric emission (see Figure S12, Supporting Information). Indeed, the corresponding frozen matrix appears visibly yellow, while the dilute fluid solution at room temperature is colorless. Contrastingly, compound **7b** displays only one structured emission at 77 K, which has been assigned to the monomeric species, indicating the lack of aggregate formation. It is clear from this set of spectroscopic data that adamantyl groups are bulky enough to effectively avoid aggregation. Complexes bearing tolyl substituents, which are planar and therefore prone to stacking, require the introduction of a bulky, branched chain on the ancillary ligand to retain the monomeric emission.

Photoluminescence spectra of neat and 10 wt % doped PMMA films (see Figure 4 and Figures S14–S21 in the Supporting Information) confirm the influence of the substituents. While the adamantyl family of compounds (**6a** and **6b**) display structured, monomeric spectra resembling homogeneous solution, it is evident that tolyl substitution (**7a** and **7b**) leads to broadened emission, proving that adamantyl moieties are useful to avoid

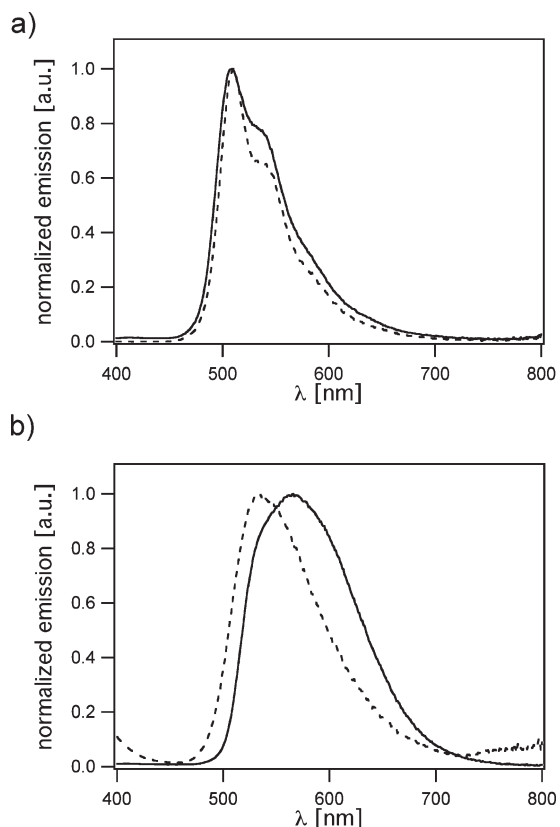


Figure 4. Emission spectra of **6a** (solid line) + **6b** (dashed line) (a) and **7a** (solid line) + **7b** (dashed line) (b) in PMMA films (10 wt %, $\lambda_{\text{exc}} = 315$ nm for **6a** and 320 nm for **7a**).

aggregation. The fact that the emission spectrum of **6b** in PMMA shows sharper vibrational features if compared with that of **6a**, and that the emission band of **7b** is narrower than that of **7a**, indicates that the introduction of branched substituents on the pyridine ancillary ligands favors the monomeric emission. Measurements in neat films further confirm these observations.

3.4. Electroluminescence Spectra. We selected compound **6a** due to the fact that it possesses the highest PLQY of the adamantyl-substituted family, which is less prone to aggregation. Vapor-processed electroluminescent devices were fabricated with the following setup: ITO/40 nm of Li224/30 nm of mCP + 6% **6a**/10 nm of ZrQ₄/60 nm of VK953/1 nm of LiF/150 nm of Al (ITO = indium tin oxide, mCP = 1,3-bis(9*H*-carbazol-9-yl)-benzene). In this setup, Li224 (4,4'-bis(dihydrodibenzazepin-1-yl)biphenyl) is a hole transporter (HOMO, -5.09 eV; LUMO, -1.65 eV) and VK953 (2,9-substituted anthracene) an electron transporter (HOMO, -6.03 eV; LUMO, -2.87 eV). Both materials are available for purchase by Sensient Imaging Technologies GmbH (see Figure S22, Supporting Information, for the chemical formulas). The electroluminescence of our best candidate was compared to that of a well-established green emitter, namely, Ir(ppy)₃, in a similar architecture.⁸⁵ The device characteristics are shown in Figure 5 and Table 3.

The aim of these tests was to observe the actual color and aggregation tendency of **6a** in a running device configuration to assess the effectiveness of our design strategy. Even though this setup is not optimized and therefore does not achieve the highest performances reported for Ir(ppy)₃, it provides a suitable way to

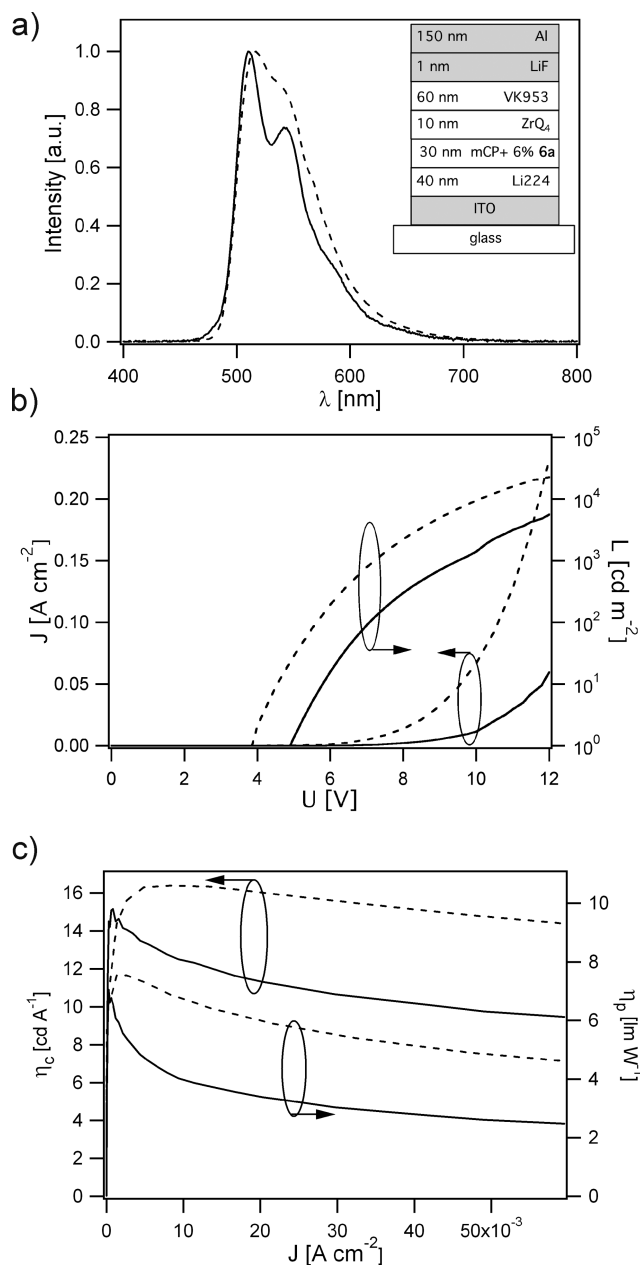


Figure 5. Device characteristics of **6a** (solid line) and Ir(ppy)₃ (dashed line) in identical device architectures: (a) electroluminescence spectra recorded at 8 V, (b) current density–voltage–luminance (J – V – L) curve, (c) luminous efficiency (η_c) and power efficiency (η_p) versus current density J .

Table 3. Device Characteristics

complex	V_{on}^a (V)	L_{max} (cd m ⁻²)	η_c (cd A ⁻¹)	η_p (lm W ⁻¹)	λ_{max} (nm)
6a	4.75	5623	15.153	7.0108	510 (1), 544 (0.74)
Ir(ppy) ₃	3.75	22545	16.394	7.5445	517 (1)

^a V_{on} = turn-on voltage.

compare the two green emitters. As can be seen in Figure 5a, compound **6a** is able to match the electroluminescence spectrum of Ir(ppy)₃. Furthermore, color purity is improved by a double-peak

emission with a maximum at 510 nm and a second one at 544 nm, which is slightly blue-shifted and more structured than the reference spectrum. It is clear that, in the running device configuration, aggregation is hindered and the clean monomer emission is retained. This is relevant for OLED applications showing that the color purity can be improved by tailoring the substitution pattern of the ligand. Comparing the device performances, a slightly higher turn-on voltage (V_{on}) relative to the reference can be observed, with 4.75 V for **6a** and 3.75 V for Ir(ppy)₃ (Figure 5b). These values are in a comparable range and show potential for optimization by using matrix materials that are tailored for each emitter. Further differences between the tested materials can be observed in Figure 5c depicting the current efficiency (η_c) and the power efficiency (η_p). On one hand, **6a** shows a maximum current efficiency of 15.2 cd A⁻¹, which is similar to the value measured for Ir(ppy)₃ (16.4 cd A⁻¹), but the efficiencies of **6a** drop at higher current densities, whereas the reference device only slightly decreases in the same range. A comparable trend is apparent in the power efficiencies, with similar maximum values at low current densities (6.8 lm W⁻¹ for **6a** and 7.5 lm W⁻¹ for the reference device). The performance of **6a** at a current density of 67 mA cm⁻² is slightly lower than that for Ir(ppy)₃, demonstrating, however, that platinum complexes with tridentate N[^]N[^]N ligands can indeed constitute interesting alternatives to iridium complexes with good color purity.

4. CONCLUSIONS

We have shown that neutral, sublimable Pt(II) complexes bearing tridentate N[^]N[^]N ligands can be designed to avoid aggregation in a running device setup, thus improving color purity. The facile synthesis and high PLQYs encourage further investigations with other substitution patterns to tune the color of the emitters in the red and blue regions of the visible spectrum.

■ ASSOCIATED CONTENT

S Supporting Information. Absorption and emission spectra, NMR spectra, illustrations of the optimized geometries for the calculated compounds, and tables containing all relevant calculated data (PDF). This material is available free of charge via the Internet at <http://pubs.acs.org>.

■ AUTHOR INFORMATION

Corresponding Author

*E-mail: ca.s@uni-muenster.de (C.A.S.); decola@uni-muenster.de (L.D.C.).

■ ACKNOWLEDGMENT

We thank the German Federal Ministry for Education and Research (BMBF) for funding, Project 13N10529 (So-Light).

■ REFERENCES

- (1) Duati, M.; Fanni, S.; Vos, J. G. *Inorg. Chem. Commun.* **2000**, 3, 68.
- (2) Duati, M.; Tasca, S.; Lynch, F. C.; Bohlen, H.; Vos, J. G.; Stagni, S.; Ward, M. D. *Inorg. Chem.* **2003**, 42, 8377.
- (3) Hage, R.; Prins, R.; Haasnoot, J. G.; Reedijk, J.; Vos, J. G. *Dalton Trans.* **1987**, 1987, 1389.
- (4) Mauro, M.; Quartapelle Procopio, E.; Sun, Y.; Chien, C.-H.; Donghi, D.; Panigati, M.; Mercandelli, P.; Mussini, P.; D'Alfonso, G.; De Cola, L. *Adv. Funct. Mater.* **2009**, 19, 2607.

- (5) Chien, C.-H.; Liao, S.-F.; Wu, C.-H.; Shu, C.-F.; Chang, S.-Y.; Chi, Y.; Chou, P.-T.; Lai, C.-H. *Adv. Funct. Mater.* **2008**, 18, 1430.
- (6) Angulo, G.; Kapturkiewicz, A.; Chang, S.-Y.; Chi, Y. *Inorg. Chem. Commun.* **2009**, 12, 378.
- (7) Carlson, B.; Eichinger, B. E.; Kaminsky, W.; Bullock, J. P.; Phelan, G. D. *Inorg. Chim. Acta* **2009**, 362, 1611.
- (8) Lee, T.-C.; Hung, J.-Y.; Chi, Y.; Cheng, Y.-M.; Lee, G.-H.; Chou, P.-T.; Chen, C.-C.; Chang, C.-H.; Wu, C.-C. *Adv. Funct. Mater.* **2009**, 19, 2639.
- (9) Vezzu, D. A. K.; Deaton, J. C.; Jones, J. S.; Bartolotti, L.; Harris, C. F.; Marchetti, A. P.; Kondakova, M.; Pike, R. D.; Huo, S. *Inorg. Chem.* **2010**, 49, 5107.
- (10) Wang, Z.; Turner, E.; Mahoney, V.; Madakuni, S.; Groy, T.; Li, J. *Inorg. Chem.* **2010**, 49, 11276.
- (11) Yang, X.; Wang, Z.; Madakuni, S.; Li, J.; Jabbour, G. E. *Adv. Mater.* **2008**, 20, 2405.
- (12) Zhou, G.; Wang, Q.; Ho, C.-L.; Wong, W.-Y.; Ma, D.; Wang, L. *Chem. Commun.* **2009**, 3574.
- (13) Williams, J. A. G. *Top. Curr. Chem.* **2007**, 281, 205.
- (14) Lu, W.; Mi, B.-X.; Chan, M. C. W.; Hui, Z.; Che, C.-M.; Zhu, N.; Lee, S.-T. *J. Am. Chem. Soc.* **2004**, 126, 4958.
- (15) Ma, B.; Djurovich, P. I.; Garon, S.; Alleyne, B.; Thompson, M. E. *Adv. Funct. Mater.* **2006**, 16, 2438.
- (16) Ma, B.; Djurovich, P. I.; Thompson, M. E. *Coord. Chem. Rev.* **2005**, 249, 1501.
- (17) Ma, B.; Li, J.; Djurovich, P. I.; Yousufuddin, M.; Bau, R.; Thompson, M. E. *J. Am. Chem. Soc.* **2005**, 127, 28.
- (18) Rochester, D.; Develay, S.; Zális, S.; Williams, J. A. G. *Dalton Trans.* **2009**, 2009, 1728.
- (19) Schneider, J.; Du, P.; Wang, X.; Brennessel, W. W.; Eisenberg, R. *Inorg. Chem.* **2009**, 48, 1498.
- (20) Unger, Y.; Zeller, A.; Taige, M.; Strassner, T. *Dalton Trans.* **2009**, 4786.
- (21) Kim, D.; Brédas, J.-L. *J. Am. Chem. Soc.* **2009**, 131, 11371.
- (22) Kwok, C.-C.; Ngai, H. M. Y.; Chan, S.-C.; Sham, I. H. T.; Che, C.-M.; Zhu, N. *Inorg. Chem.* **2005**, 44, 4442.
- (23) Li, M.; Chen, W.-H.; Lin, M.-T.; Omary, M. A.; Shepherd, N. D. *Org. Electron.* **2009**, 10, 863.
- (24) Develay, S.; Blackburn, O.; Thompson, A. L.; Williams, J. A. G. *Inorg. Chem.* **2008**, 47, 11129.
- (25) D'Andrade, B.; Brooks, J.; Adamovich, V.; Thompson, M. E.; Forrest, S. *Adv. Mater.* **2002**, 14, 1032.
- (26) Hudson, Z. M.; Sun, C.; Helander, M. G.; Amarné, H.; Lu, Z.-H.; Wang, S. *Adv. Funct. Mater.* **2010**, 20, 3426.
- (27) Cho, J.-Y.; Domercq, B.; Barlow, S.; Suponitsky, K. Y.; Li, J.; Timofeeva, T. V.; Jones, S. C.; Hayden, L. E.; Kimyonok, A.; South, C. R.; Weck, M.; Kippelen, B.; Marder, S. R. *Organometallics* **2007**, 26, 4816.
- (28) Cocchi, M.; Kalinowski, J.; Fattori, V.; Williams, J. A. G.; Murphy, L. *Appl. Phys. Lett.* **2009**, 94, 073309.
- (29) Cummings, S.; Eisenberg, R. *J. Am. Chem. Soc.* **1996**, 118, 1949.
- (30) Chang, S.-Y.; Cheng, Y.-M.; Chi, Y.; Lin, Y.-C.; Jiang, C.-M.; Lee, G.-H.; Chou, P.-T. *Dalton Trans.* **2008**, 6901.
- (31) Chang, S.-Y.; Kavitha, J.; Li, S.-W.; Hsu, C.-S.; Chi, Y.; Yeh, Y.-S.; Chou, P.-T.; Lee, G.-S.; Carty, A. J.; Tao, Y.-T.; Chien, C.-H. *Inorg. Chem.* **2006**, 45, 137–146.
- (32) Chan, S.-C.; Chan, M. C. W.; Wang, Y.; Che, C.-M.; Cheung, K.-K.; Zhu, N. *Chem.—Eur. J.* **2001**, 7, 4180.
- (33) Adamovich, V.; Brooks, J.; Tamayo, A.; Alexander, A. M.; Djurovich, P. I.; D'Andrade, B. W.; Adachi, C.; Forrest, S. R.; Thompson, M. E. *New J. Chem.* **2002**, 26, 1171.
- (34) Elbejrani, O.; Rashdan, M. D.; Nesterov, V.; Rawashdeh-Omary, M. A. *Dalton Trans.* **2010**, 39, 9465.
- (35) Garg, J. A.; Blacque, O.; Fox, T.; Venkatesan, K. *Inorg. Chem.* **2010**, 49, 11463.
- (36) Armaroli, N.; Accorsi, G.; Cardinali, F.; Listorti, A. *Top. Curr. Chem.* **2007**, 280, 69.

- (37) Chowdhury, S.; Patra, G. K.; Drew, M. G. B.; Chattopadhyay, N.; Datta, D. *Dalton Trans.* **2000**, 235.
- (38) Miller, A. J. M.; Dempsey, J. L.; Peters, J. C. *Inorg. Chem.* **2007**, *46*, 7244.
- (39) Benedix, R.; Hennig, H.; Kunkely, H.; Vogler, A. *Chem. Phys. Lett.* **1990**, *175*, 483.
- (40) Chang, K.-H.; Huang, C.-C.; Liu, Y.-H.; Hu, Y.-H.; Chou, P.-T.; Lin, Y.-C. *Dalton Trans.* **2004**, 1731.
- (41) Deda, M.; Ghedini, M.; Aiello, I.; Grisolia, A. *Chem. Lett.* **2004**, *33*, 1060.
- (42) Ferguson, J.; Krausz, E. *Inorg. Chem.* **1987**, *26*, 1383.
- (43) Gui-ying, D.; Wen-long, J.; Jin, W.; Li-Zhong, W.; Guang-de, W.; Lin, C.; Xin-hua, O.; He-Ping, Z. *Semicond. Sci. Technol.* **2009**, *24*, 025016.
- (44) Highland, R. G.; Brummer, J. G.; Crosby, G. A. *J. Phys. Chem.* **1986**, *90*, 1593.
- (45) Ho, K.-Y.; Yu, W.-Y.; Cheung, K.-K.; Che, C.-M. *Dalton Trans.* **1999**, 1999, 1581.
- (46) Liu, Q.-D.; Wang, R.; Wang, S. *Dalton Trans.* **2004**, 2004, 2073.
- (47) Roh, S.-G.; Kim, Y.-H.; Seo, K. D.; Lee, D. H.; Kim, H. K.; Park, Y.-I.; Park, J.-W.; Lee, J.-H. *Adv. Funct. Mater.* **2009**, *19*, 1663.
- (48) Sapochak, L. S.; Benincasa, F. E.; Schofield, R. S.; Baker, J. L.; Riccio, K. K. C.; Fogarty, D.; Kohlmann, H.; Ferris, K. F.; Burrows, P. E. *J. Am. Chem. Soc.* **2002**, *124*, 6119.
- (49) Son, H.-J.; Han, W.-S.; Chun, J.-Y.; Kang, B.-K.; Kwon, S.-N.; Ko, J.; Han, S. J.; Lee, C.; Kim, S. J.; Kang, S. O. *Inorg. Chem.* **2008**, *47*, 5666.
- (50) Vellis, P. D.; Mikroyannidis, J. A.; Lo, C.-N.; Hsu, C.-S. *J. Polym. Sci., Part A* **2008**, *46*, 7702.
- (51) Zhang, H.-Y.; Ye, K.-Q.; Zhang, J.-Y.; Liu, Y.; Wang, Y. *Inorg. Chem.* **2006**, *45*, 1745.
- (52) Develay, S.; Williams, J. A. G. *Dalton Trans.* **2008**, 4562.
- (53) Tang, R. P.-L.; Wong, K. M.-C.; Zhu, N.; Yam, V. W.-W. *Dalton Trans.* **2009**, 2009, 3911.
- (54) Jarosz, P.; Lotito, K.; Schneider, J.; Kumaresan, D.; Schmehl, R.; Eisenberg, R. *Inorg. Chem.* **2009**, *48*, 2420.
- (55) Zhang, H.; Zhang, B.; Li, Y.; Sun, W. *Inorg. Chem.* **2009**, *48*, 3617.
- (56) Tam, A. Y.-Y.; Wong, K. M.-C.; Yam, V. W.-W. *J. Am. Chem. Soc.* **2009**, *131*, 6253.
- (57) Williams, J. A. G. *Chem. Soc. Rev.* **2009**, *38*, 1783.
- (58) Williams, J. A. G.; Beeby, A.; Davies, E. S.; Weinstein, J. A.; Wilson, C. *Inorg. Chem.* **2003**, *42*, 8609.
- (59) Farley, S. J.; Rochester, D. L.; Thompson, A. L.; Howard, J. A. K.; Williams, J. A. G. *Inorg. Chem.* **2005**, *44*, 9690.
- (60) Shao, P.; Li, Y.; Azenkeng, A.; Hoffmann, M. R.; Sun, W. *Inorg. Chem.* **2009**, *48*, 2407.
- (61) Schneider, J.; Du, P.; Jarosz, P.; Lazarides, T.; Wang, X.; Brennessel, W. W.; Eisenberg, R. *Inorg. Chem.* **2009**, *48*, 4306.
- (62) Strassert, C. A.; Chien, C.-H.; Galvez Lopez, M. D.; Kourkoulos, D.; Hertel, D.; Meerholz, K.; De Cola, L. *Angew. Chem., Int. Ed.* **2011**, *50*, 946.
- (63) Yuen, M.-Y.; Roy, V. A. L.; Lu, W.; Kui, S. C. F.; Tong, G. S. M.; So, M.-H.; Chui, S. S.-Y.; Muccini, M.; Ning, J. Q.; Xu, S. J.; Che, C. *Angew. Chem., Int. Ed.* **2008**, *47*, 9895.
- (64) Lu, W.; Chui, S. S.-Y.; Ng, K.-M.; Che, C.-M. *Angew. Chem., Int. Ed.* **2008**, *47*, 4568.
- (65) Lu, W.; Chen, Y.; Roy, V. A. L.; Chui, S. S.-Y.; Che, C.-M. *Angew. Chem., Int. Ed.* **2009**, *48*, 7621.
- (66) Chen, Y.; Li, K.; Lu, W.; Chui, S. S.-Y.; Ma, C.-W.; Che, C.-M. *Angew. Chem., Int. Ed.* **2009**, *48*, 9909.
- (67) Perdew, J. P.; Burke, K.; Ernzerhof, M. *Phys. Rev. Lett.* **1996**, *77*, 3865.
- (68) Perdew, J. P.; Burke, K.; Ernzerhof, M. *Phys. Rev. Lett.* **1997**, *78*, 1396.
- (69) Adamo, C.; Barone, V. *J. Chem. Phys.* **1999**, *110*, 6158.
- (70) Francl, M. M.; Pietro, W. J.; Hehre, W. J.; Binkley, J. S.; Gordon, M. S.; DeFrees, D. J.; Pople, J. A. *J. Chem. Phys.* **1982**, *77*, 3654.
- (71) Stratmann, R. E.; Scuseria, G. E.; Frisch, M. J. *J. Chem. Phys.* **1998**, *109*, 8218.
- (72) Casida, M. E.; Jamorski, C.; Casida, K. C.; Salahub, D. R. *J. Chem. Phys.* **1998**, *108*, 4439.
- (73) Gaussian 09, Revision B.1; Frisch, M. J.; Trucks, G. W.; Schlegel, H. B.; Scuseria, G. E.; Robb, M. A.; Cheeseman, J. R.; Scalmani, G.; Barone, V.; Mennucci, B.; Petersson, G. A.; Nakatsuji, H.; Caricato, M.; Li, X.; Hratchian, H. P.; Izmaylov, A. F.; Bloino, J.; Zheng, G.; Sonnenberg, J. L.; Hada, M.; Ehara, M.; Toyota, K.; Fukuda, R.; Hasegawa, J.; Ishida, M.; Nakajima, T.; Honda, Y.; Kitao, O.; Nakai, H.; Vreven, T.; Montgomery, J. A., Jr.; Peralta, J. E.; Ogliaro, F.; Bearpark, M.; Heyd, J. J.; Brothers, E.; Kudin, K. N.; Staroverov, V. N.; Kobayashi, R.; Normand, J.; Raghavachari, K.; Rendell, A.; Burant, J. C.; Iyengar, S. S.; Tomasi, J.; Cossi, M.; Rega, N.; Millam, J. M.; Klene, M.; Knox, J. E.; Cross, J. B.; Bakken, V.; Adamo, C.; Jaramillo, J.; Gomperts, R.; Stratmann, R. E.; Yazyev, O.; Austin, A. J.; Cammi, R.; Pomelli, C.; Ochterski, J. W.; Martin, R. L.; Morokuma, K.; Zakrzewski, V. G.; Voth, G. A.; Salvador, P.; Dannenberg, J. J.; Dapprich, S.; Daniels, A. D.; Farkas, O.; Foresman, J. B.; Ortiz, J. V.; Cioslowski, J.; Fox, D. J. Gaussian, Inc.: Wallingford, CT, 2009.
- (74) The corresponding ^{13}C NMR spectrum of the monomer could not be measured due to aggregation of the compound at the concentration necessary for this measurement. These characteristics will be discussed in a separate publication.
- (75) Orselli, E.; Kottas, G. S.; Konradsson, A. E.; Coppo, P.; Fröhlich, R.; De Cola, L.; van Dijken, A.; Büchel, M.; Börner, H. *Inorg. Chem.* **2007**, *46*, 11082.
- (76) Bard, A. J.; Faulkner, L. R. *Electrochemical Methods, Fundamentals and Applications*, 2nd ed.; Wiley: New York, 2001.
- (77) Brooks, J.; Babayan, Y.; Lamansky, S.; Djurovich, P. I.; Tsyba, I.; Bau, R.; Thompson, M. E. *Inorg. Chem.* **2002**, *41*, 3055.
- (78) Danilov, E. O.; Rachford, A. A.; Goeb, S.; Castellano, F. N. *J. Phys. Chem. A* **2009**, *113*, 5763.
- (79) Garner, K. L.; Parkes, L. F.; Piper, J. D.; Williams, J. A. G. *Inorg. Chem.* **2010**, *49*, 476.
- (80) Hua, F.; Kinayyigit, S.; Cable, J. R.; Castellano, F. N. *Inorg. Chem.* **2006**, *45*, 4304.
- (81) Rachford, A. A.; Hua, F.; Adams, C. J.; Castellano, F. N. *Dalton Trans.* **2009**, 2009, 3950.
- (82) Hirani, B.; Li, J.; Djurovich, P. I.; Yousufuddin, M. *Inorg. Chem.* **2007**, *46*, 3865.
- (83) Hua, F.; Kinayyigit, S.; Rachford, A. A.; Shikhova, E. A.; Goeb, S.; Cable, J. R.; Adams, C. J.; Kirschbaum, K.; Pinkerton, A. A.; Castellano, F. N. *Inorg. Chem.* **2007**, *46*, 8771.
- (84) Wang, K.-W.; Chen, J.-L.; Cheng, Y.-M.; Chung, M.-W.; Hsieh, C.-C.; Lee, G.-H.; Chou, P.-T.; Chen, K.; Chi, Y. *Inorg. Chem.* **2010**, *49*, 1372.
- (85) Baldo, M. A.; Lamansky, S.; Burrows, P. E.; Thompson, M. E.; Forrest, S. R. *Appl. Phys. Lett.* **1999**, *75*, 4.